Lapped transforms and hidden Markov models for seismic data filtering

Laurent Duval, Caroline Chaux

International Journal of Wavelets, Multiresolution and Information Processing

Lapped transforms and hidden Markov models for seismic data filtering*

Laurent DUVAL
Technology, Computer Science and Applied Mathematics Department,
Institut Français du Pétrole,
92500 Rueil-Malmaison Cedex, France
laurent.duval@ifp.fr

Caroline CHAUX
Institut G. Monge, Université de Marne-la-Vallée
77454 Marne-la-Vallée, France
caroline.chaux@univ-mlv.fr

Received (Day Month Year)
Revised (Day Month Year)
Communicated by (xxxxxxxxxx)

Seismic exploration provides information about the ground substructures. Seismic images are generally corrupted by several noise sources. Hence, efficient denoising procedures are required to improve the detection of essential geological information. Wavelet bases provide sparse representation for a wide class of signals and images. This property makes them good candidates for efficient filtering tools, allowing the separation of signal and noise coefficients. Recent works have improved their performance by modelling the intra- and inter-scale coefficient dependencies using hidden Markov models, since image features tend to cluster and persist in the wavelet domain. This work focuses on the use of lapped transforms associated with hidden Markov modelling. Lapped transforms are traditionally viewed as block-transforms, composed of M pass-band filters. Seismic data present oscillatory patterns and lapped transforms oscillatory bases have demonstrated good performances for seismic data compression. A dyadic like representation of lapped transform coefficient is possible, allowing a wavelet-like modelling of coefficients dependencies. We show that the proposed filtering algorithm often outperforms the wavelet performance both objectively (in terms of SNR) and subjectively: lapped transform better preserve the oscillatory features present in seismic data at low to moderate noise levels.

Keywords: seismic data filtering; lapped transforms; hidden Markov models.

AMS Subject Classification: 22E46, 53C35, 57S20

*This work has been partly presented to the *Wavelets and Statistics Conference*, Sep. 4–7, 2003, Grenoble, France.

1. Introduction

Seismic exploration aims at providing information about the ground substructures. This information is addressed indirectly by disturbances, artificially created by seismic energy sources. The disturbances propagate through the ground, where geophysical strata reflect the spreading wave front. Portions of the reflected (or refracted) waves are then collected by sensors, often situated near the ground surface. The one-dimensional signal acquired by a single sensor is called a seismic trace. In the simplest convolutive earth model, a trace is a time-based signal composed of the generated disturbance convolved with the reflection coefficients at the strata interfaces. Seismic processing is the task of inferring substructures location and properties from the collected signals, with the help of geological models. Seismic signals generally decrease in energy as the wave front propagates deeper and are scattered by subsurface heterogeneities. The signals are also corrupted by several noise sources that reduce the possibility to detect essential information such as strata or faults. Seismic data filtering is thus a prominent task in seismic processing, especially as exploration aims at imaging deeper targets, in geologically disturbed zones.

Although the term *wavelet*(from the French *ondelette*, or little wave[1]) was originally used in seismic for the short support dirac shaped disturbance, wavelets have re-emerged only recently in geophysics as efficient compression[2] and noise filtering tools[3].

1.1. *Related work*

Due to the large volumes of seismic data, the discrete wavelet transform (DWT) has generally been preferred to its continuous integral counterpart. Some authors have nevertheless remarked that, although seismic traces usually appear as naturally made of physical wavelets, seismic images are sometimes more efficiently represented by other short local bases. It as been shown in the context of compression with lapped transforms[4] (LT) seen as filter banks or with the Local Cosine Transform[5] (LCT). These short local bases are believed to be more efficient at capturing seismic oscillatory patterns, which bear some similarities with textures in natural images. A comparison of various local cosine transforms for image compression is given in[6].

Going back to about more than 15 years of developments, the discrete wavelet transform provides sparse bases for natural signal and images. As a consequence, numerous DWT-based algorithms have been proposed in the past years for efficient signal and image statistical analysis. For instance, wavelet-domain thresholding or shrinkage is known to provide asymptotically optimal performance[7] in the case of gaussian additive noise. One of the key to noise filtering is to transform the signal and the noise to a domain where their statistics are modelled more efficiently, via appropriate (often orthogonal) transforms. But it has been quickly remarked that a mere scalar coefficient thresholding after transformation did not yield the best results in practical implementations. More specifically, several authors have

observed that wavelet decompositions exhibit two heuristic properties often termed as "clustering" and "persistence": feature-related wavelet coefficients (near edges or singularities) tend to *cluster* locally in a subband and to *persist* across scales, through the classical wavelet parent-child quad-tree structure. Recently, algorithms adopted tree-adapted subband-dependent shrinkage[8,9]. Also, sophisticated models of the joint statistics may be useful for capturing key-features in real-world images. Recent approaches rely on Markov random fields. We refer to L. Rabiner[10] and A. Willsky[11] for an rich overview of their use in signal and image processing.

Recently, M. Crouse *et al.*[12,13] have proposed a new framework based on the hidden Markov tree. Based on[12], H. Choi *et al.*[14] have proposed efficient image denoising[15] as well as robust SAR segmentation[16]. HMM-based algorithms seem to take more advantage of the "clustering" and "persistence" properties of wavelet coefficients around image features. They yield an improved modelling of the coefficients' statistical dependencies and their non Gaussian behavior. They have recently been notably improved by their use in the context of texture segmentation with dual-tree complex wavelets[17] and steerable pyramids[18].

1.2. *Main contribution*

We propose in the present work to extend the use of hidden Markov models to a lapped transform domain for seismic data filtering. This work has been partly presented in[19]. LT are usually viewed as block-transforms, composed of M pass-band filters. The superiority of lapped transforms over wavelets may come from additional design flexibility and short local bases.

Lapped transforms were generally not often used in compression on denoising algorithms, due to the superiority of the inter-scale coefficient dependency obtained from the wavelet dyadic decomposition. Though, T. Tran *et al.*[20] have demonstrated that well-designed LT are able to improve on DWT for natural image compression, in the Embedded Zero-tree framework[21]. In the context of denoising, the LT coefficients are rearranged into an octave-like representation. The resulting "scales" bear the same clustering and persistence properties as in the wavelet representation. Moreover, LT design may enforce both orthogonality and linear-phase (in contrast to non-Haar 1D wavelets), as well as attractive additional degrees of freedom in design.

The superiority of lapped transforms over wavelets may come from these design degrees of freedom and sharper frequency attenuation properties of the M filters (potentially reducing aliasing effects across the subbands). One other interesting feature is based on Z. Xiong *et al.*[22]: the dyadic remapping property. When the number of channels M is a power of 2, the transformed coefficients may be rearranged into an octave-like representation. Experiments demonstrate that the resulting "scales" still bear interesting clustering and persistence properties, while keeping superior oscillatory pattern preservation.

As a consequence, we propose here to use hidden Markov models with lapped

transforms, relying on[12,15]. Special care is taken in the design of the LT used, to assess the anisotropic shape of some seismic surveys.

In the following, we first address the philosophy behind the recently developed wavelet-domain hidden Markov models in Section 2. Then, we focus on the combination of lapped transforms and hidden Markov models in Section 3, where lapped transforms design and properties are reviewed, as well as the dyadic representation of block transforms. Section 4 briefly describes properties of seismic data with an emphasis on their oscillatory nature. Objective and subjective denoising results are discussed in Section 5. Finally, we draw some conclusions on the proposed lapped transform based hidden Markov model denoising algorithm, as well as possible improvements.

2. Wavelet-Domain Hidden Markov Models

Under the additive noise assumption, an image x and its noisy observation x^n are usually written as

$$x^n(i,j) = x(i,j) + n(i,j)\,, \tag{2.1}$$

where n is a random noise. The joint probability density function of the family of images that x belongs to is often unattainable. Based on wavelet approximate decorrelation, simpler models have been proposed for coefficient modelling. The simplest independent Gaussian models generally obtain improvements from residual inter-coefficients dependencies.

M. Crouse *et al.*[12] have recently proposed a new framework for statistical signal processing, based on wavelet-domain hidden Markov models (WD-HMM).

Let $w_{j,k}$ denote a wavelet coefficient at level j, $1 \leq j \leq J$, with $j = 1$ corresponding to the coarsest wavelet scale. The marginal *pdf* for the associated random variable W is modelled as a Gaussian mixture of N_S components. In the framework of hidden Markov models[23], a discrete hidden state $S_{j,k}$ is associated to each $w_{j,k}$ with a probability mass function $P(S_{j,k} = s)$ given for each state s, $1 \leq s \leq N_S$. While the values $w_{j,k}$ are observed, the value of the state S is generally unknown. Depending on the actual state s the coefficient, the conditional *pdf* of W given $S = s$ is given by $f_{W|S}(w|S = s)$, modelled as a Gaussian distribution, described in Eq. 2.2:

$$g_s(w; \mu^s_{j,k}, \sigma^s_{j,k}) = \frac{1}{\sqrt{2\pi}\sigma^s_{j,k}} \exp\left(-\left(\frac{w - \mu^s_{j,k}}{\sigma^s_{j,k}}\right)^2\right) \tag{2.2}$$

where μ_x and σ_x^2 are the mean and the variance of g. The *pdf* of W is given by:

$$p_W(w_{j,k}) = \sum_{s=1}^{N_S} P(S_{j,k} = s) f_{W|S}(w|S = s)\,. \tag{2.3}$$

Based on heuristics developed for image compression[21], the most widely used model considers a two-state HMM, where the wavelet coefficients are considered as

belonging to either a large $\mathcal{L}$ or small $\mathcal{S}$ state depending on whether the coefficient is located near a discontinuity or not. The associated probabilities $p_{\mathcal{L}} = p_j^1$ (the superscript 1 referring to the root node) and $p_{\mathcal{S}} = 1 - p_j^1$ possess large and small variances respectively. Since the coefficients w are obtained by pass-band or high-pass filters, they are assumed to have zero mean. The model can be further reduced by considering that the variances are constant across each scale j, for a given state s. As a consequence, Eq. 2.3 results in the following marginal distribution:

$$p_W(w_{j,k}) = \sum_{s \in \{\mathcal{L},\mathcal{S}\}} p_s g_s(0, \sigma_{j,.}^s)\,. \tag{2.4}$$

The HMT (hidden Markov tree) model is often described as a quad-tree structured probabilistic graph that captures the statistical properties of the wavelet transform of images. The HMT materializes the cross-scale link between the hidden states. It draws inspiration from zero-tree or hierarchical trees image compression systems[21,24]. An illustration of an HMT is depicted in Figure 1.

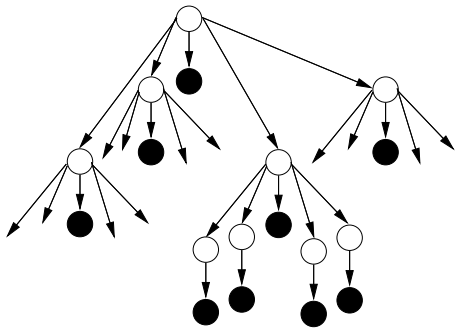

Fig. 1. Diagram of a hidden Markov tree in a quad-tree. White dots represent hidden states with arrows as dependencies, black dots the transformed coefficients. The black dot on the top represents a parent coefficient with its four children.

The persistence property is modelled by a markovian dependency between parent and children hidden states at consecutive scales. A state S_j associated with the child coefficient $w_{j,k}$ at scale j depends only on the state $S_{\rho(j)}$ of its parent coefficient $w_{\rho(j)}$ at scale $j-1$. The transition probabilities between the two states s_1 (parent) and s_2 (child) can be described by the transition matrix ϵ_j, given by:

$$\epsilon_{j,\rho(j)}^{s_1 \to s_2} = p_{S_j|S_{\rho(j)}}(S_j = s_2 | S_{\rho(j)} = s_1),\ s_1, s_2 \in \{\mathcal{L}, \mathcal{S}\}. \tag{2.5}$$

The WD-HMT is completely defined by the set Θ of model parameters:

$$\Theta = \{p_j^1, \epsilon_2, \ldots, \epsilon_J, \sigma_{j,.}^s\},\ 1 \le j \le J,\ s \in \{\mathcal{L}, \mathcal{S}\}. \tag{2.6}$$

The resulting statistical model is able to capture efficiently the joint parent-child and the marginal distributions of the transformed coefficients. There exists efficient

Expectation Maximization algorithms for fitting a HMT using the Minimum Length Description criterion. We refer to[12,15,25] for details on the implementation of hidden Markov trees.

3. Lapped transforms and HMT models

3.1. *Generalities on Lapped Transforms*

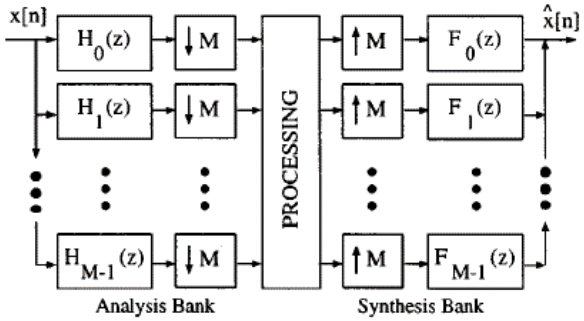

Fig. 2. Block diagram of a M-channel maximally decimated filter bank ($H_k(z)$: analysis and $F_k(z)$: *synthesis*).

The Lapped Orthogonal Transform[26] (LOT) has been developed to overcome annoying blocking artifacts arising from non overlapping block transforms such as the Discrete Cosine Transform. More generally, lapped transforms are defined as linear phase paraunitary filter banks (FB). Figure 2 shows a typical M-channel maximally decimated filter bank. The kth analysis and synthesis subband filters are denoted by $H_k(z)$ and $F_k(z)$, respectively. The filter bank may be efficiently represented by its polyphase form by $\mathbf{E}(z)$ (type-I analysis polyphase matrix) and $\mathbf{R}(z)$ (type-II synthesis polyphase matrix), defined by:

$$[H_0(z)\, H_1(z)\, \ldots\, H_{M-1}(z)]^{\mathrm{T}} = \mathbf{E}(z^M) \left[1\, z^{-1}\, \ldots\, z^{1-M}\right]^{\mathrm{T}}. \tag{3.7}$$

and

$$[F_0(z)\, F_1(z)\, \ldots\, F_{M-1}(z)] = \left[z^{1-M}\, z^{2-M}\, \ldots\, 1\right] \mathbf{R}(z^M). \tag{3.8}$$

The analysis and the synthesis M-band FB polyphase matrices $\mathbf{R}(z)$ and $\mathbf{E}(z)$ (represented in Fig. 3) provide perfect reconstruction with zero delay if and only if:

$$\mathbf{R}(z)\mathbf{E}(z) = \mathbf{I}_M\,, \tag{3.9}$$

where $\mathbf{I}_M$ is the identity matrix[27]. LT may be parameterized through efficient lattice structures for cost-driven optimization. We refer to [26,27,20] for a comprehensive overview on lapped transforms. If we restrict ourselves to a subset of lapped transforms with:

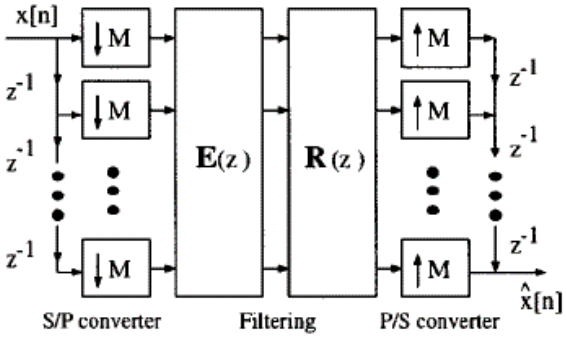

Fig. 3. Block diagram of the M-channel maximally decimated filter bank from Fig. 2 with polyphase implementation.

- an even number M of channels;
- FIR filters with linear phase and length L multiple of M $(L = KM)$;

a large class of LT, called Generalized Lapped Biorthogonal Transforms (GLBT) may be rewritten in the following form: let U_i and V_i be invertible matrices, Φ_i and W defined for $i \in 1, \ldots, n$ as:

$$\Phi_i = \begin{bmatrix} U_i & 0 \\ 0 & V_i \end{bmatrix} , \tag{3.10}$$

$$W = \begin{bmatrix} I & I \\ I & -I \end{bmatrix} , \tag{3.11}$$

$$\Lambda(z) = \begin{bmatrix} I & \\ & z^{-1}I \end{bmatrix} , \tag{3.12}$$

$$K_0 = \Phi_0 W \text{ , and } K_i(z) = \frac{1}{2}\Phi_i W \Lambda(z) W . \tag{3.13}$$

Then the analysis polyphase matrix can be factored as:

$$E(z) = \prod_{K-1}^{0} K_i(z) , \tag{3.14}$$

with an appropriate choice of invertible matrices U_i and V_i. The inverse synthesis polyphase matrix follows by element-wise inversion of matrices in Formula 3.10–3.13.

3.2. *Lapped transform optimization*

The degrees of freedom in the design of lapped transforms reside in the invertible matrices U_i and V_i. It is well known that the Givens decomposition splits any given

orthogonal matrix of size $M/2 \times M/2$ in a product of $M(M-2)/8$ elementary rotations [28] . In addition, every invertible matrix U can be factored into the product $U_l U_\Delta U_r$, where U_l and U_r are two orthogonal matrices and U_Δ is a diagonal matrix with non-negative elements Δ_i. Such a decomposition is summarized in Figure 4 for a 4×4 invertible matrix.

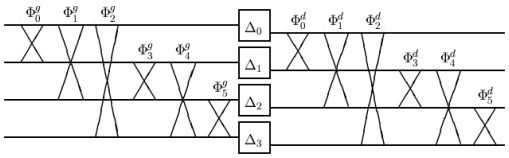

Fig. 4. Givens decomposition of an 4×4 invertible matrix U.

Sparse transforms are generally desired for signal denoising. It is also desirable to design transforms with reduced aliasing in the transform domain. Transforms can be obtained using unconstrained non-linear optimization of a weighted sum of popular cost criteria for compression: generalized coding gain G_c, stop-band attenuation for the analysis and synthesis filter bank A^a_{sb} and A^s_{sb}, DC leakage A_{dc} and attenuation at mirror frequencies A_{mf}, detailed in Equations 3.15–3.19.

$$G_c = 10 \log \left[\prod_{i=0}^{M-1} \left(\frac{\sigma_{x_i}}{\sigma_x} \left\| F_i \right\|_2 \right)^2 \right]^{-1/M} , \tag{3.15}$$

$$A^a_{\mathrm{sb}} = \sum_{i=0}^{M-1} \int_{\omega \in \Omega_i} \left| H_i \left(e^{j\omega} \right) \right|^2 d\omega \, , \tag{3.16}$$

$$A^s_{\mathrm{sb}} = \sum_{i=0}^{M-1} \int_{\omega \in \Omega_i} \left| F_i \left(e^{j\omega} \right) \right|^2 d\omega \, , \tag{3.17}$$

$$A_{\mathrm{dc}} = \left| \sum_{i=2,4,\ldots}^{M-1} \sum_{j=0}^{L-1} H_i \left(j \right) \right| , \tag{3.18}$$

$$A_{\mathrm{mf}} = \sum_{i=0}^{M-1} \left| H_i \left(e^{j\omega_i} \right) \right|^2 . \tag{3.19}$$

We refer to[20] for details on LT optimization. It was shown in[4] that a lapped transform optimization allowed superior seismic data compression results, as compared to wavelet coding, as proposed by P. Donoho *et al.*[2]. Since seismic images generally exhibit anisotropic features (cf. Section 4), it is desirable to use different transforms for the horizontal and the vertical dimensions of the image. In this work, we use the traditional AR(1) intersample autocorrelation coefficient ρ model in the

joint optimization of the coding gain and the other cost criteria. Different ρ are estimated for different types of seismic data, in both the horizontal and vertical direction.

3.3. *Dyadic remapping of Lapped Transforms*

Since hidden Markov tree models are based on a quad-tree structure, their use in a lapped transform framework requires a similar arrangement for the LT coefficients. A LT projects signals onto M equally spaced frequency bands, in contrast to the octave-band wavelet representation. Fortunately, such a arrangement is possible if the number of channels M is a power of 2 (typically 8 or 16). The transformed coefficients bear an octave-like grouping, with $J = \log_2 M$ decomposition levels[22]. In one dimension, for one group of M transformed coefficients, the DC component (corresponding to the average of the signal coefficients) is assigned to the lower scale subband. Then, from low to high frequencies, the kth subband is formed respectively from the next group of $2^k/2$ coefficients. The $J+1$ groups are then associated with respect to the block position in the signal. Figure 5 illustrates the dyadic rearrangement for two consecutive blocks of $M = 8$ coefficients. The two blocks of $8 = 2^3$ coefficients (dots on top of Figure 5) are rearranged into $J+1 = 4$ groups and yield a three-level decomposition (dots on bottom of Figure 5). In two

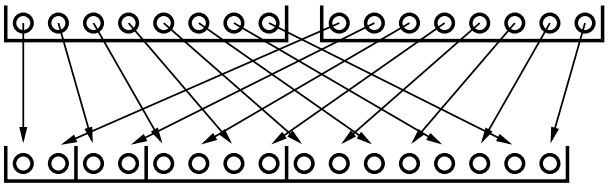

Fig. 5. Dyadic rearrangement of 1D LT coefficients: (Top) block-transform with uniform frequency partition, (Bottom) octave-like representation.

dimensions, the re-mapping from a four channel block transform to a two level dyadic transform is depicted in Fig. 6. The right-hand side image is made of 8×8 sub-blocks. Each sub-block gathers 4×4 coefficients (see the top left sub-block), where the black squares represent the DC components. In a fashion similar to the 1D case, all the 64 DC coefficients are grouped into a 8×8 square (top left of the left-hand side image) representing the low-pass component of the dyadic representation. Arrows between coefficients link reciprocal locations of coefficients in the dyadic and the block grouping scheme. Once wavelet and LT coefficients share similar grouping, similar denoising algorithms may be applied to both domains.

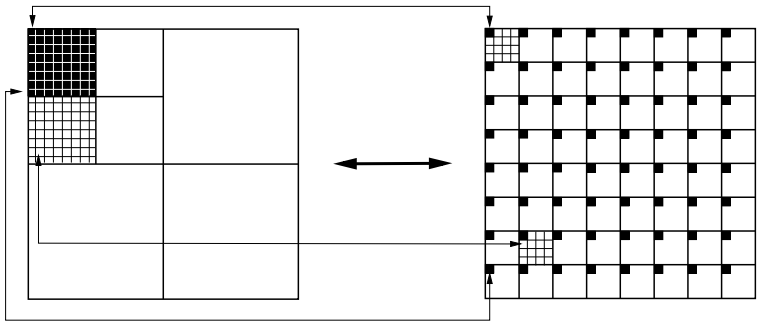

Fig. 6. Dyadic equivalence between 2D wavelet and LT coefficients: (Left) two-level octave-like representation, (Right) four-channel block-transform with uniform frequency partition.

4. Generalities on Seismic Data

Seismic exploration aims at providing information about the ground substructures. This information is indirectly addressed by disturbances, artificially created by seismic energy sources. The disturbances propagate through the ground, where geophysical strata reflect the spreading wave front. Portions of the reflected (or refracted) waves are then collected by sensors (geophones, represented by squares in Fig. 7), often situated near the ground surface. The one-dimensional signal acquired by a single sensor is called a seismic trace. In the simplest convolutive earth model, a trace is a time-based signal made of the generated disturbance convolved with the reflection coefficients at the strata interfaces. The reflection and acquisition of seismic signals is represented on Figure 7. Disturbances provoked by the seismic source (depicted by triangles on Fig. 7) propagate along the ray-paths (represented by dashed lines). Each location on the reflector is illuminated by several propagations between couples of source and receptor.

Seismic processing is the task of inferring substructure location and properties from the collected signals, with the help of geological models. Seismic signals generally decrease in energy as the wave front propagates deeper and is scattered by subsurface heterogeneities. The signals are also corrupted several noise sources that reduce the possibility to detect essential information such as strata or faults. Seismic data filtering is thus a prominent task in seismic processing, especially as exploration aims at imaging deeper targets, in geologically disturbed zones. We refer to the book by Ö. Yilmaz[29] for a comprehensive survey on seismic processing.

In this work, lapped transform based HMT filtering is applied on the two dimensional seismic image represented in 8. It has been tailored to 512×512 samples. The left panel represents each signal sample as a pixel, similarly to traditional images. The right panel displays each column as a wiggle plot. The later is often used in geophysics to emphases on layers. It is obtained through the processing of a collec-

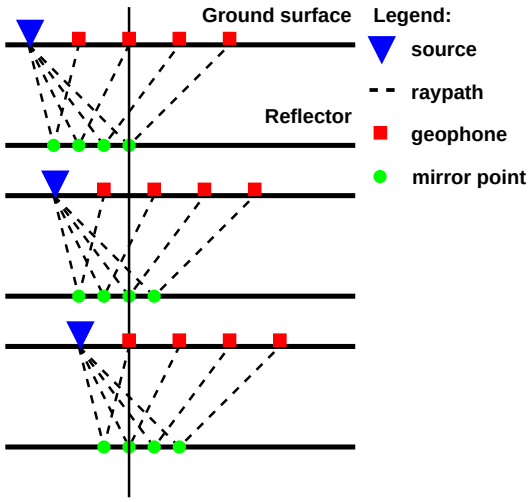

Fig. 7. Seismic acquisition for one horizontal layer and three different shot points.

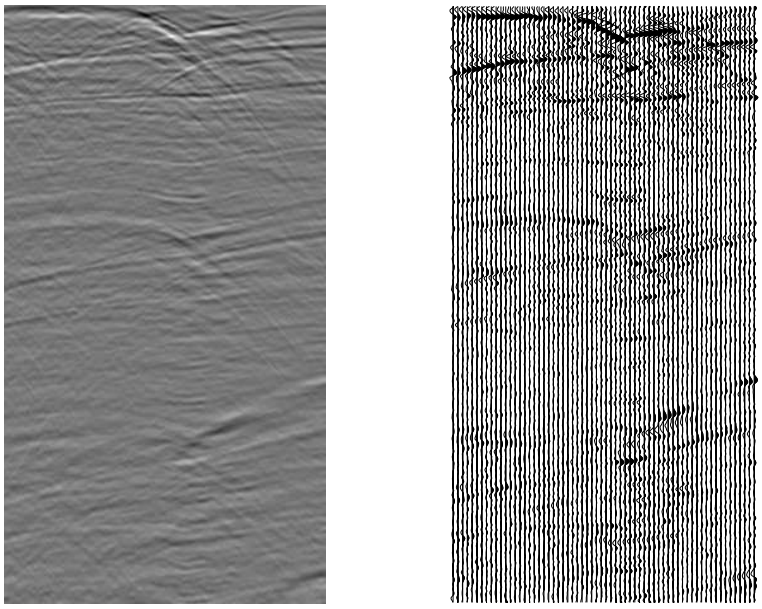

Fig. 8. Example of stacked seismic data in classical image form (left) and with a wiggle plot (right).

tion of seismic traces. The horizontal direction corresponds to the spatial extend of the seismic survey. The vertical direction coarsely reflects the combined response of several seismic traces sharing common reflection location on geological strata.

Figure 8 thus provides a section of the ground substructure. The vertical direction is a function of time, since it depends on the time of arrival of the wave front to each sensor. It is not corrected with the velocity in each strata, and thus does not provide directly information on the depth of the substructures. Figure 9 depicts the first vertical trace obtained from Figure 8. The oscillatory behavior of seismic data clearly appears from Figure 9. It justifies the use of transforms capable of capturing these oscillations. The crossings appearing on the seismic image are zones of interest, which shall not be blurred by denoising procedures. The decomposition coefficients magnitude for the 30-tap orthogonal Coiflet and a 32-tap lapped transform, for one vertical signal, are depicted in Figure 10, from the low-pass to the high-pass subband (left to right). Figure 11 displays the same coefficients, sorted by decreasing magnitude. We remark that the smallest coefficients (on the right hand side) with the Lapped Transform are substantially smaller than that of the wavelet (dotted blue). This behavior illustrates how a lapped transform yields a sparser decomposition, with generally less large and more small coefficients. The sparsity of the transform is illustrated in 2D in 12–14.

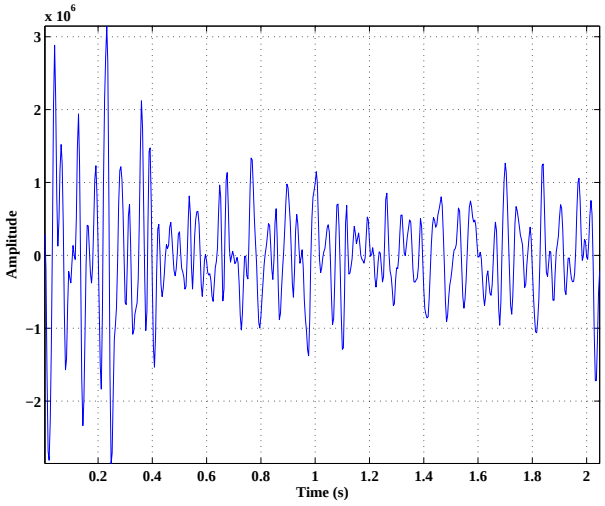

Fig. 9. First seismic trace (vertical direction) from Fig. 8.

5. Experimental results

5.1. *Comments on the dyadic remapping*

Figures 12–14 illustrate the effects of decomposition on the seismic data. The transformed coefficients c_k are rescaled by a geometrical factor following $\mathrm{sign}(c_k)|c_k|^{\alpha}$ for display purposes.

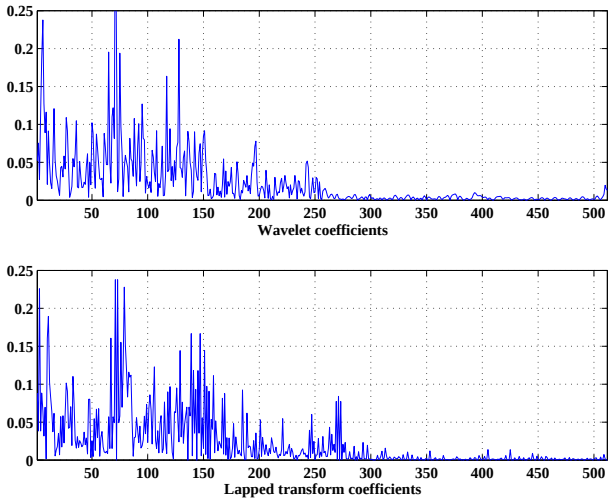

Fig. 10. Wavelet and lapped transform coefficients obtained from the decomposition of the signal from Fig. 9.

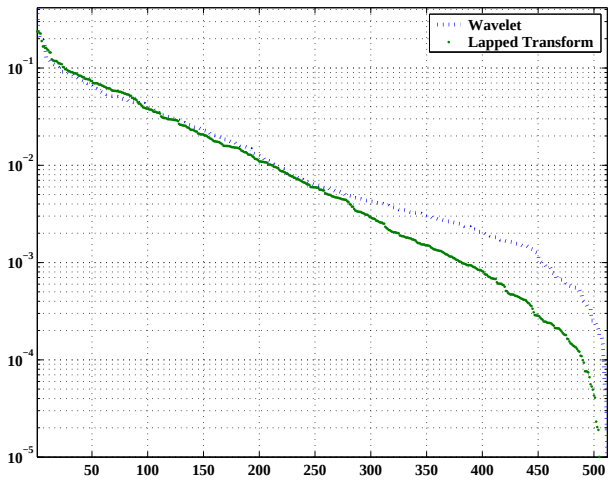

Fig. 11. Wavelet and lapped transform coefficients from Fig. 10, sorted in decreasing order.

Figure 12 represents the decomposition with a 30-tap orthogonal Coiflet filter bank. The top left corner is the low-pass approximation of the image. The other subbands exhibit the horizontal and diagonal structures of the data in the highest frequency bands. Almost no features are present in the vertical subbands, due to the directions present in the image. They exhibit mostly incoherent coefficients due

to the noise. Figure 13 represents the block-wise decomposition of seismic data (see the diagram on the right of Fig. 6). The transformed coefficients are rearranged in Figure 14. Compared to Figure 12, this representation exhibits less high magnitude coefficients (bright dots), yielding a sparser decomposition. The anisotropic content of the seismic image suggests that separate models can be used for the horizontal, diagonal and vertical subbands of the wavelet tree, in contrast to what is observed in natural images, for instance in M. Do *et al.*[18], where it is suggested that wavelet coefficients at the same scale and location but different orientations should be tied up together to have the same hidden state.

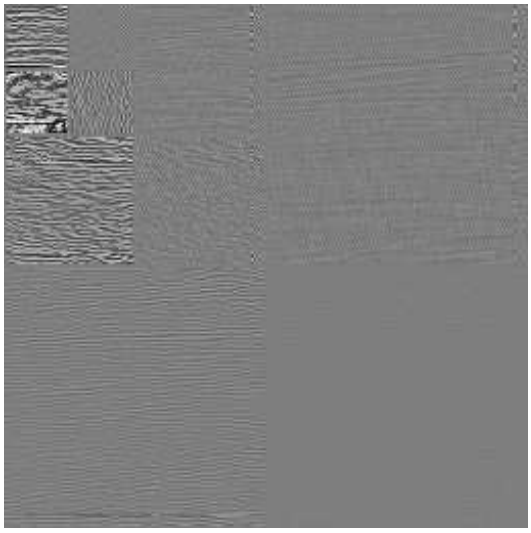

Fig. 12. Dyadic representation of seismic data from Fig. 8 obtained from a three-level wavelet decomposition (Coiflet 30-tap filters).

5.2. *Choice of the lapped transform*

The experimental results presented here have been obtained with an eight-channel 32-tap orthogonal lapped transform. Its basis vectors are represented in Figure 15. This structure have been optimized using the cost functions described in Section 3.2. Different AR(1) models are derived from the horizontal and vertical directions of the seismic data, to account for the different correlation dependencies in both directions. An eight-channel lapped transform yields a three-level dyadic after remapping. The resulting low-pass approximation is further decomposed by a wavelet transform. Results are compared in Section 5 with a wavelet decomposition at the same level. The same wavelet is used in both cases.

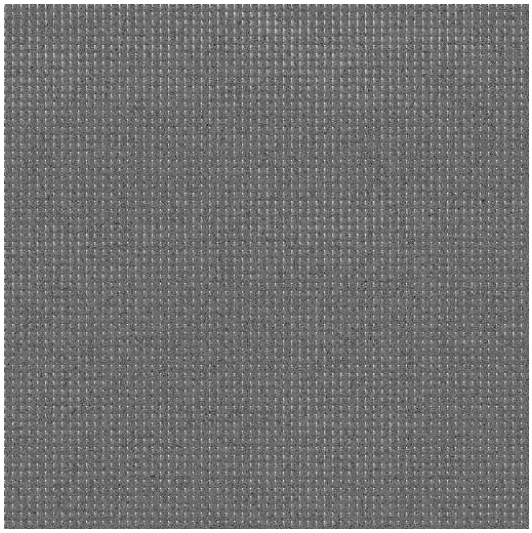

Fig. 13. Block representation of seismic data from Fig. 8 obtained from a eight-channel lapped transform.

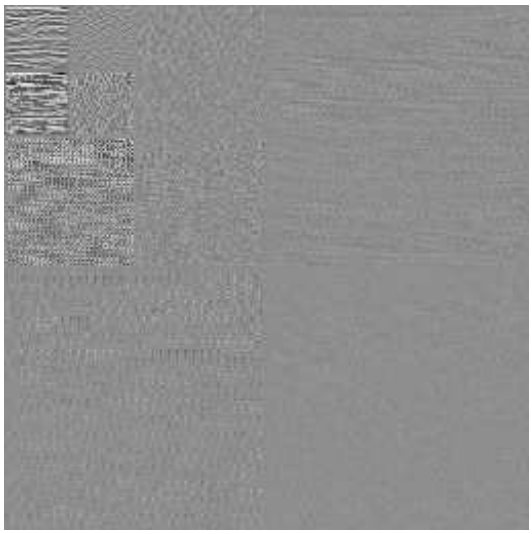

Fig. 14. Dyadic representation of seismic data from Fig. 8 obtained from a eight-channel lapped transform (Fig. 13 after dyadic remapping).

5.3. *Results*

The denoising results are addressed in both the objective and subjective sense. Objective results are described in terms of signal-to-noise ratio (SNR): let s_k, s_k^n,

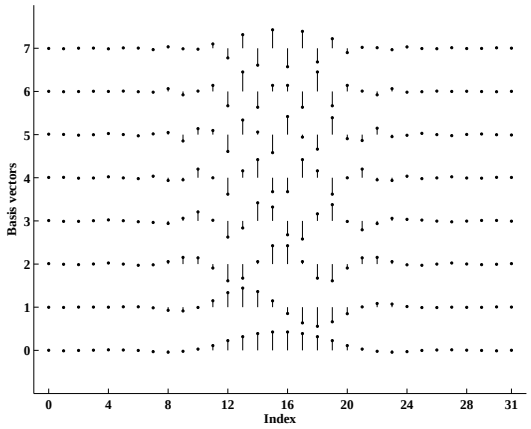

Fig. 15. Basis vectors for an eight-channel 32-tap orthogonal lapped transform .

s_k^d be the samples of the original, the noisy and the denoised data respectively.

$$\mathrm{SNR} = 20 \log_{10} \left(\sum_k \frac{s_k^2}{(s_k - s_k^d)^2} \right) . \tag{5.20}$$

Table 1. Objective denoising results comparison at various initial signal-to-noise levels in dB.

Noisy data	Wavelet (Coif 30)[a]	LT (8×32)[b]
21.9	30.1	29.9
24.4	31.7	32.1
26.0	32.7	33.2
29.1	34.8	35.3
34.0	38.3	39.0
40.0	42.4	43.2
43.0	44.6	45.4

Note: Table notes
[a] Two-channel 30-tap Coiflet filter bank
[b] Eight-channel 32-tap orthogonal lapped transform

The original data is corrupted by gaussian white noise at various levels. Table 1 gathers SNR results after denoising for both the wavelet and the lapped transform HMT noise removal. We should mention that denoising results typically vary within ± 0.1 dB with different noise realizations at the same variance. Both HMT-based algorithms provide up to 8 dB improvement at low SNRs. This gap decreases as the SNR increases. Lapped transform based denoising exhibits a slight superiority in terms of signal-to-noise ratio, which does not exceed 1.0 dB with this data.

Subjective results also are of specific importance for seismic data quality assessment. It is particularly important that denoising does not blur the ground substructure. Therefore, it is useful to carefully observe the denoised data, as well as the noise removed by the filtering procedure, as illustrated in Figures 16–19. Each figure represents the denoised data s_k^d (left panel) and the removed noise (or difference section), *i.e.* $s_k^n - s_k^d$, on the right panel. The major requirements are that features remain clear in the denoised image and that the difference section exhibits as few structured noise as possible.

Figures 16–17 display the denoised images with an initial moderate 40 dB noise. Clearer structure preservation is apparent at the top of the seismic section after lapped transform denoising: the utmost top alignments on the seismic image have apparently merged after wavelet denoising. This feature is more pronounced (more coherent on neighboring traces) on the wavelet denoised difference section. We conclude that at moderate SNRs, lapped transforms generally preserve seismic information better that wavelets, while objective measures do not differ by more than 1 dB.

Seismic features preservation is clearer at lower SNRs, as illustrated in Figures 18–19. Oversmoothing is observed after wavelet denoising on the left of 19, especially at the bottom of the image. Crest and valley alignments in the wiggles align less evidently than in the LT case. Difference sections from Figures 18–19 (right hand side) clearly show that a lot more of structured information is removed with wavelet, as compared to lapped transform denoising. Similar observations were derived on texture preservation in natural images[30]. Textures and seismic seem to share similar oscillatory content, giving an advantage on lapped transform decomposition over wavelet bases for denoising.

6. Conclusions and discussion

We propose to extend the use of hidden Markov models to a lapped transform domain for seismic data filtering. Lapped transforms are converted to a dyadic like representation, to account for inter-scale coefficient dependencies. Due to the oscillatory nature of seismic data, oscillatory projection bases yield sparer decomposition of the data. Moreover, lapped transform enjoy improved design degrees of freedom. They allow to design data adapted transforms. Sharper attenuation between the filter frequency bands also reduces aliasing effects in the frequency domain. We show that lapped transform based denoising generally outperforms wavelet denoising using an objective SNR measure. More important, we demonstrate that lapped transforms better preserve seismic information (subjectively), since they cause less blurring than wavelet and the removed noise contains less coherent geologic structures.

For fair comparison, we used the same decomposition level for the wavelet and the lapped transform. Since the decomposition is limited with the LT, depending on the number of channels, it is further split by applying a wavelet decomposition

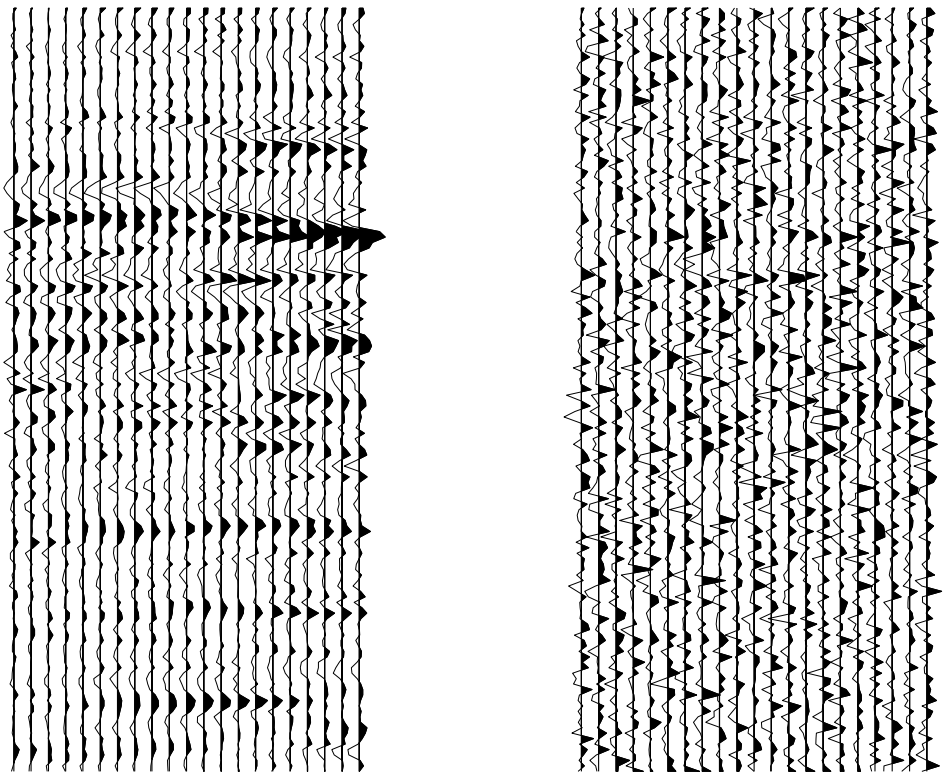

Fig. 16. Seismic image (left) and difference section (right) with lapped transform based HMT denoising at 40.0 dB.

to the low-pass subband. Future works will focus on a better control of the low-pass approximation image, possibly by a hierarchical lapped transform with shorter support, to reduce edge artifacts on the smaller approximation. Improvement is also possible with the use of more involved directional transforms or shift-invariant implementation, since the lapped transforms used in this work are maximally decimated.

Acknowledgment

The first author would like to thank H. Elloumi for programming some of the filter bank routines used in this work.

References

1. P. Goupillaud, A. Grossmann, and J. Morlet. Cycle-octave and related transforms in seismic signal analysis. *Geoexploration*, 23:85–102, 1984/85.
2. P. L. Donoho, R. A. Ergas, R. S. Polzer, and J. D. Villasenor. Compression opti-

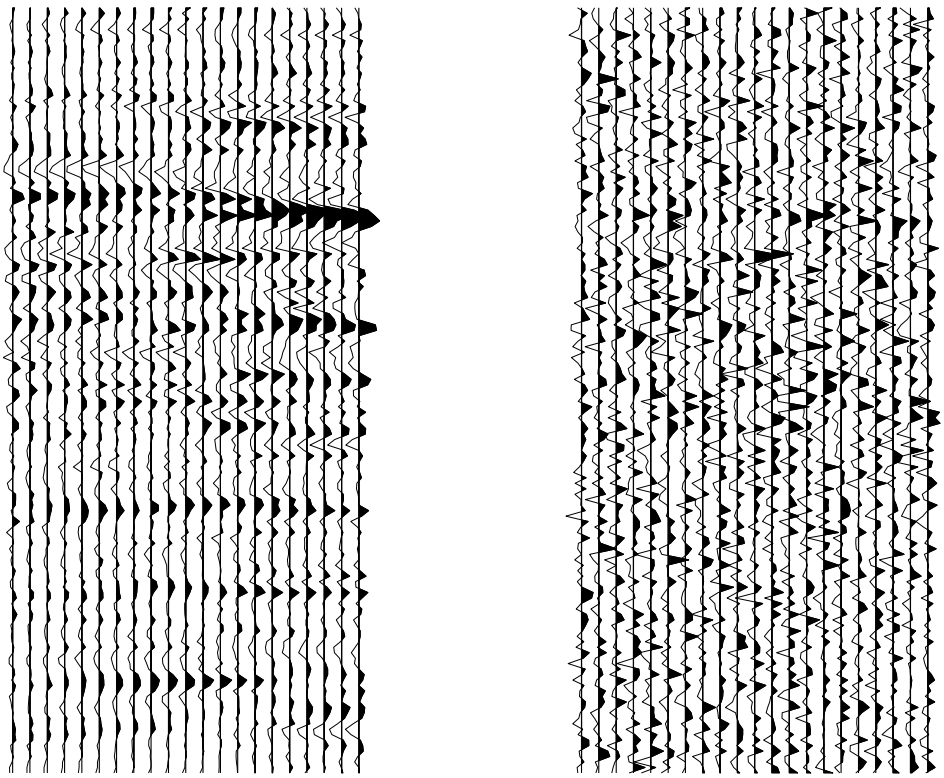

Fig. 17. Seismic image (left) and difference section (right) with wavelet based HMT denoising at 40.0 dB.

mization by multidimensional wavelet transforms and data dependent quantization. In *Annual International Meeting*, volume 2, page 2042. Soc. of Expl. Geophysicists, 1996. Exp. abstracts.

3. N. Saito. Simultaneous noise suppression and signal compression using a library of orthogonal bases and the minimum description length criterion. In E. Foufoula-Georgiu and P. Kumar, editors, *Wavelets in Geophysics*, pages 299–324. Academic Press, Inc., 1994.
4. L. C. Duval, T. Q. Nguyen, and T. D. Tran. On progressive seismic data compression using GenLOT. In *Proc. 33rd Conf. on Information Sciences and Systems*, Mar. 1999.
5. A. Averbuch, R. Coifman, F. Meyer, J.-O. Stromberg, and A. Vassiliou. Low bit-rate efficient compression for seismic data. *IEEE Trans. on Image Proc.*, pages 1801–1814, Dec. 2001.
6. F. G. Meyer. Image comparison with adaptive local cosines: A comparative study. *IEEE Trans. Image Processing*, 11(6):616–629, 2002.
7. D. L. Donoho. De-noising by soft-thresholding. *IEEE Trans. on Inform. Theory*, 41(3):613–627, May 1995.
8. S. G. Chang, B. Yu, and M. Vetterli. Adaptive wavelet thresholding for image denoising and compression. *IEEE Trans. on Image Proc.*, 9(9):1532–1546, Sep. 2000.

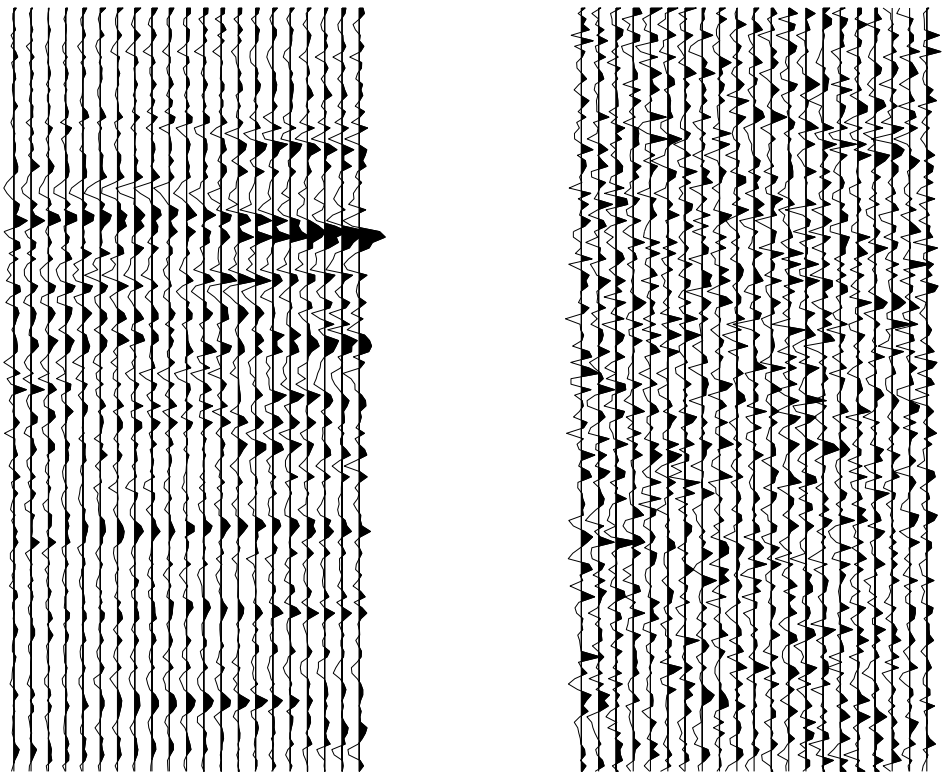

Fig. 18. Seismic image (left) and difference section (right) with lapped transform based HMT denoising at 23.1 dB.

9. S. Walker and Y.-J. Chen. Image denoising using tree-based wavelet subband correlations and shrinkage. *Opt. Eng.*, 39(11):2900–2908, November 2000.
10. Lawrence R. Rabiner. A tutorial on Hidden Markov Models and selected applications in speech recognition. *Proc. IEEE*, 77(2):257–286, Feb. 1989.
11. A. Willsky. Multiresolution Markov models for signal and image processing. *Proc. IEEE*, 90(8):1396–1458, August 2002.
12. M. Crouse, R. Nowak, and R. Baraniuk. Wavelet-based signal processing using hidden Markov models. *IEEE Trans. on Signal Proc.*, 46(4):886–902, April 1998.
13. Robert D. Nowak. Multiscale hidden Markov models for bayesian image analysis. Technical Report MSU-ENGR-004-98, Michigan State University, 1998.
14. H. Choi, J. Romberg, R. Baraniuk, and N. Kingbury. Hidden Markov tree modeling of complex wavelet tranforms. In *Proc. Int. Conf. on Acoust., Speech and Sig. Proc.*, 2000.
15. J. Romberg, H. Choi, and R. Baraniuk. Bayesian tree-structured image modeling using wavelet-domain hidden Markov models. In *Proc. SPIE Technical Conference on Mathematical Modeling, Bayesian Estimation, and Inverse Problems*, pages 31–44, 1999.
16. V. Venkatachalam, H. Choi, and R. Baraniuk. Multiscale SAR image segmenta-

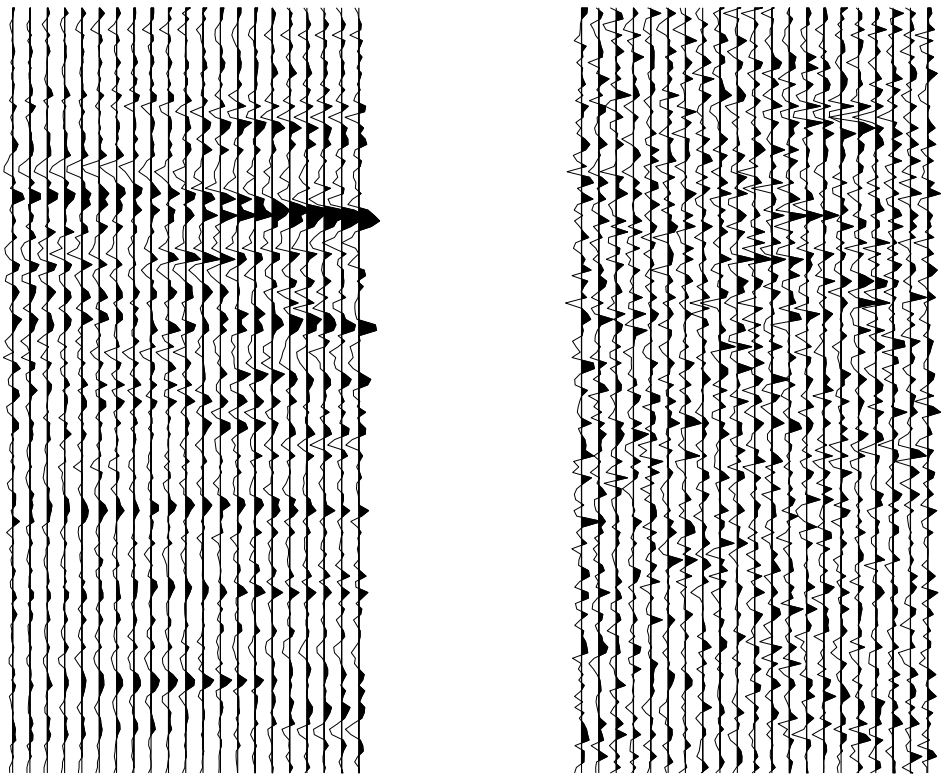

Fig. 19. Seismic image (left) and difference section (right) with wavelet based HMT denoising at 23.1 dB.

tion using wavelet-domain hidden Markov tree models. In *Proc. SPIE Symposium on Aerospace/Defense Sensing, Simulation, and Controls, Algorithms for Synthetic Aperture Radar Imagery VII*, 2000.

17. J. H. Won, K. Pyun, and R. M. Gray. Hidden Markov multiresolution texture segmentation using complex wavelets. In *Proc. Int. Conf. on Telecommunications*, pages 1624–1630, 2003.
18. M. N. Do and M. Vetterli. Rotation invariant texture characterization and retrieval using steerable wavelet-domain hidden Markov models. *IEEE Trans. on Multimedia*, Dec. 2002.
19. L. Duval and C. Chaux. Seismic data filtering with lapped transforms and hidden Markov models. In *Proc. Wavelet and Statistics*, 2003. Abstracts.
20. T. D. Tran, R. L. de Queiroz, and T. Q. Nguyen. Linear phase perfect reconstruction filter bank: lattice structure, design, and application in image coding. *IEEE Trans. on Signal Proc.*, 48:133–147, January 2000.
21. Jerome M. Shapiro. Embedded image coding using zerotrees of wavelet coefficients. *IEEE Trans. on Signal Proc.*, 41:3445–3462, Dec. 1993.
22. Z. Xiong, O. Guleryuz, and Michael T. Orchard. A DCT-based embedded image coder. *IEEE Signal Processing Letters*, November 1996.

23. Pierre Brémaud. *Markov chains, Gibbs fields, Monte Carlo simulation and queues.* Springer Verlag, 1999.
24. A. Said and W. A. Pearlman. A new fast/efficient image codec based on Set Partitioning in Hierarchical Trees. *IEEE Trans. on Circ. and Syst. for Video Technology*, 6:243–250, June 1996.
25. J.-B. Durand and P. Gonçalvès. Statistical inference for hidden Markov tree models and application to wavelet trees. Technical Report N 4248, INRIA, Sept. 2001.
26. Henrique S. Malvar. *Signal Processing with Lapped Transforms.* Artech House, 1992.
27. G. Strang and T. Nguyen. *Wavelets and Filter Banks.* Wellesley-Cambridge Press, Wellesley, MA, 1996.
28. R. A. Horn and C. R. Johnson. *Matrix analysis.* Cambridge University Press, 1985.
29. Özdogan Yilmaz. *Seismic data analysis.* Society of Exploration Geophysicists, 2nd edition, 2001.
30. L. Duval and T. Q. Nguyen. Lapped transform domain using hidden Markov trees. In *Proc. Int. Conf. on Image Processing*, 2003.